AFRL-RX-WP-JA-2015-0091

THERMAL AND OXIDATION RESPONSE OF UHTC LEADING EDGE SAMPLES EXPOSED TO SIMULATED HYPERSONIC FLIGHT CONDITIONS (POSTPRINT)

Michael K. Cinibulk
AFRL/RXCC

Triplicane A. Parthasarathy and Melvin D. Petry
UES, Inc.

Tarun Mathur
ISSI

Mark R. Gruber
AFRL/RQHF

MARCH 2013
Interim Report

AIR FORCE RESEARCH LABORATORY
MATERIALS AND MANUFACTURING DIRECTORATE
WRIGHT-PATTERSON AIR FORCE BASE OH 45433-7750
AIR FORCE MATERIEL COMMAND
UNITED STATES AIR FORCE

NOTICE AND SIGNATURE PAGE

Using Government drawings, specifications, or other data included in this document for any purpose other than Government procurement does not in any way obligate the U.S. Government. The fact that the Government formulated or supplied the drawings, specifications, or other data does not license the holder or any other person or corporation; or convey any rights or permission to manufacture, use, or sell any patented invention that may relate to them.

Qualified requestors may obtain copies of this report from the Defense Technical Information Center (DTIC) (http://www.dtic.mil).

AFRL-RX-WP-JA-2015-0091 HAS BEEN REVIEWED AND IS APPROVED FOR PUBLICATION IN ACCORDANCE WITH ASSIGNED DISTRIBUTION STATEMENT.

//Signature//

PATRICK S. CARLIN, Project Engineer
Composite Materials and Processing Section
Composite Branch
Structural Materials Division

//Signature//

SEAN C. COGHLAN, Chief
Composite Materials and Processing Section
Composite Branch
Structural Materials Division

//Signature//

ROBERT T. MARSHALL, Deputy Chief
Structural Materials Division
Materials And Manufacturing Directorate

This report is published in the interest of scientific and technical information exchange and its publication does not constitute the Government's approval or disapproval of its ideas or findings.

REPORT DOCUMENTATION PAGE

Form Approved
OMB No. 0704-0188

1. REPORT DATE *(DD-MM-YY)*	2. REPORT TYPE	3. DATES COVERED *(From - To)*
March 2013	Interim	1 February 2013 – 12 February 2013

4. TITLE AND SUBTITLE
THERMAL AND OXIDATION RESPONSE OF UHTC LEADING EDGE SAMPLES EXPOSED TO SIMULATED HYPERSONIC FLIGHT CONDITIONS (POSTPRINT)

5a. CONTRACT NUMBER
In-house

5b. GRANT NUMBER

5c. PROGRAM ELEMENT NUMBER
62102F

6. AUTHOR(S)
See back

5d. PROJECT NUMBER
4347

5e. TASK NUMBER

5f. WORK UNIT NUMBER
X0S7

7. PERFORMING ORGANIZATION NAME(S) AND ADDRESS(ES)
See back

8. PERFORMING ORGANIZATION REPORT NUMBER

9. SPONSORING/MONITORING AGENCY NAME(S) AND ADDRESS(ES)
Air Force Research Laboratory
Materials and Manufacturing Directorate
Wright-Patterson Air Force Base, OH 45433-7750
Air Force Materiel Command
United States Air Force

10. SPONSORING/MONITORING AGENCY ACRONYM(S)
AFRL/RXCC

11. SPONSORING/MONITORING AGENCY REPORT NUMBER(S)
AFRL-RX-WP-JA-2015-0091

12. DISTRIBUTION/AVAILABILITY STATEMENT
Distribution Statement A. Approved for public release; distribution unlimited.

13. SUPPLEMENTARY NOTES
Journal article published in *Journal of the American Ceramic Society*, 96 [3] 907-915. ©2010 The American Ceramic Society. The U.S. Government is joint author of the work and has the right to use, modify, reproduce, release, perform, display or disclose the work. This report contains color. The final publication is available at DOI:10.1111/jace.12180.

14. ABSTRACT

Sharp Leading Edge (LE) samples of UHTC (20 vol%SiC–HfB2) and SiC were exposed to simulated hypersonic flight conditions using a direct-connect scramjet rig and their thermal and oxidation responses measured. The measured backwall temperatures and scale thicknesses were significantly smaller than might be expected from stagnation temperatures at the LE. Furthermore, the scale that formed around the LE was more uniform than expected from the steep drop in cold wall heat flux with distance from the tip. These results were interpreted and rationalized using physics-based models. An aerothermal model in combination with an oxidation model accounted for the observed scale thicknesses at the tip and their slight variation with distance. The scale thicknesses were similar to values reported for exposures in furnaces at temperatures calculated for the tip, but less than those reported in arc jet tests. The formation of Hafnon (HfSiO4) and the absence of external glassy layer and of silica in the outer portions of the oxide region are unique to scramjet tested samples, presumably due to the high fluid flow (high shear and evaporation) rates.

15. SUBJECT TERMS
leading edge, UHTC, SiC, hypersonic, aerothermal model, oxidation, ICMSE

16. SECURITY CLASSIFICATION OF:			17. LIMITATION OF ABSTRACT:	18. NUMBER OF PAGES	19a. NAME OF RESPONSIBLE PERSON (Monitor)
a. REPORT	b. ABSTRACT	c. THIS PAGE			Patrick S. Carlin
Unclassified	Unclassified	Unclassified	SAR	13	19b. TELEPHONE NUMBER *(Include Area Code)* (937) 904-5547

REPORT DOCUMENTATION PAGE Cont'd

6. AUTHOR(S)

Michael K. Cinibulk - AFRL/RXCC

Triplicane A. Parthasarathy and Melvin D. Petry - UES, Inc.

Tarun Mathur – ISSI

Mark R. Gruber - AFRL/RQHF

7. PERFORMING ORGANIZATION NAME(S) AND ADDRESS(ES)

AFRL/RXCC
2941 Hobson Way
Bldg 654, RM 136
Wright-Patterson AFB OH 45433

UES Inc.
4401 Dayton-Xenia Rd.
Dayton, OH 45432-1894

ISSI
Dayton, Ohio

AFRL/RQHF
1950 5th Street
Wright-Patterson AFB OH 45433

journal

J. Am. Ceram. Soc., 96 [3] 907–915 (2013)
DOI: 10.1111/jace.12180

Thermal and Oxidation Response of UHTC Leading Edge Samples Exposed to Simulated Hypersonic Flight Conditions

Triplicane A. Parthasarathy,[‡,§,†] Melvin D. Petry,[‡,§] Michael K. Cinibulk,[‡] Tarun Mathur,[¶] and Mark R. Gruber[‖]

[‡]Air Force Research Laboratory, Materials and Manufacturing Directorate, Wright-Patterson AFB 45433-7817, Ohio

[§]UES, Inc., Dayton 45432, Ohio

[¶]ISSI, Dayton, Ohio

[‖]Air Force Research Laboratory, Aerospace Systems Directorate, Wright-Patterson AFB, Ohio

Sharp leading edge (LE) samples of UHTC (20 vol%SiC–HfB_2) and SiC were exposed to simulated hypersonic flight conditions using a direct-connect scramjet rig and their thermal and oxidation responses measured. The measured back-wall temperatures and scale thicknesses were significantly smaller than might be expected from stagnation temperatures at the LE. Furthermore, the scale that formed around the LE was more uniform than expected from the steep drop in cold wall heat flux with distance from the tip. These results were interpreted and rationalized using physics-based models. An aerothermal model in combination with an oxidation model accounted for the observed scale thicknesses at the tip and their slight variation with distance. The scale thicknesses were similar to values reported for exposures in furnaces at temperatures calculated for the tip, but less than those reported in arc jet tests. The formation of hafnon ($HfSiO_4$) and the absence of external glassy layer and of silica in the outer portions of the oxide region are unique to scramjet tested samples, presumably due to the high fluid flow (high shear and evaporation) rates.

I. Introduction

The cowl (LE) and fuel injection struts of a scramjet engine present two critical materials challenges in the development of reusable hypersonic flight vehicles. Both are required to have, and retain during flight, a sharp curvature (762 μm or 30 mil radius in current design) while bearing the extreme conditions of hypersonic flow. The conditions experienced by a sharp body under hypersonic flow conditions have been the subject of modeling since the early 1950s.[1–3] It is widely recognized that environmental resistance is important for this application.[4–6] Key parameters that represent these conditions with respect to material survivability are heat flux, total or stagnation temperature, total or stagnation pressure, dynamic pressure, fluid velocity near the material surface behind the bow shock, fluid composition, the degree of dissociation of gaseous elements and catalytic recombination at the material's surface. In addition, resistance to environmental attack, vibrations, and thermal shock will also be important. However, the difficulty in reproducing these conditions has precluded a proper evaluation of materials for this application. Most of the experiments, that study potential candidate materials, are conducted in a laboratory furnace, thus assigning the total temperature as the key parameter by default.[5,7–15] Alternately it is possible to use a laser as a heat source where candidate materials are evaluated by comparing performance under a calculated cold wall heat flux, and in some cases with imposed fluid flow.[16,17] The arc-heater or arc-jet test, originally developed to simulate atmospheric reentry, is sometimes used to evaluate materials for hypersonic applications, by reproducing a calculated enthalpy.[6,18–21] However, the heat flux in these tests varies depending on the material surface-dependent catalytic coefficient for recombination of gases. Finally, testing using real hypersonic flights is very expensive and thus rare.[22]

We recently reported that using a scramjet rig samples can be tested under conditions that simulate to a reasonable accuracy free-flight conditions.[23] This test reproduces the same heat flux, total temperature, stagnation pressure, and fluid velocity behind the bow shock as experienced in free flight at an altitude of 25 km. Its key limitation is that the gas chemistry is different from air, with lower oxygen and higher moisture and carbon-dioxide levels.[5] Among the candidate materials that are expected to survive these conditions are ultra-high temperature ceramics (UHTC) made of ZrB_2 or HfB_2 with 20 vol% SiC, which have been shown to have good oxidative stability up to 2000°C.[5–13,24–32]

In this work, experiments were conducted that explored the thermal and oxidation responses of LE samples made of two material choices, UHTC and SiC, subjected to the simulated hypersonic conditions of Mach numbers ranging from 4 to 7 at an altitude of 25 km. The thermal and oxidation responses of the samples were measured, modeled, and compared to responses in furnace tests and arc jet tests reported in the literature to help interpret/rationalize all of the observations.

II. Experimental Procedure

The LE samples were wedge-shaped with a 762 μm (30 mils) radius of curvature and a 12° included angle [Fig. 1(a)], as per design guidelines for current scramjet for reusable application. The UHTC sample was electro discharge machined from SPS (Spark Plasma Sintering) processed material of composition 20 vol% SiC–HfB_2, as described in Ref. 15 The SiC sample was sintered SiC (Hexaloy SE, St Gobain, Niagara Falls, NY) that was machined (diamond ground) by a commercial vendor (Bomas Machine Specialties, Inc., Somerville, MA). The details of the direct-connect scramjet rig used in this work can be found in Refs. 33,34 Briefly, it is a scramjet engine built to study supersonic combustion over a range of simulated flight

J. Smialek—contributing editor

Manuscript No. 32023. Received September 18, 2012; approved December 11, 2012.
†Author to whom correspondence should be addressed. email: Triplicane.Parthasarathy@wpafb.af.mil

conditions. The rig is supplied with compressed air that is heated using a combustion heater to stagnation temperatures simulating flight conditions over a range of Mach numbers from 3 to 7, at dynamic pressures up to 95.8 kPa. The combustion heater is fueled with natural gas; oxygen is added in sufficient quantities such that the oxygen mole fraction of the test gas matches that of clean air. A supersonic nozzle then accelerates the test gas to the proper Mach number at the entrance to the scramjet engine. The resulting supersonic flow enters the combustion section where ethylene is used as fuel. The combustor exhaust gases have an enthalpy that is equivalent to free stream hypersonic flow. It must be clarified that the gas flow rate itself is supersonic and not hypersonic, although the enthalpy content is the same as hypersonic flow thus simulating free flight at Mach numbers up to 7. The facility includes a variety of conventional and advanced instrumentation for accurate documentation of combustor inlet and exit conditions. The rig has been calibrated to obtain profiles of pitot pressure, total temperature, and wall static pressure distributions for a wide range of inlet conditions. In addition, combustion fluid dynamics modeling of the rig has been conducted to obtain predicted conditions within the rig, and found to be in good agreement with experiments.[33,34] As shown in our prior work,[23] it is possible to suspend leading edge samples in the combustor exit flow path of the scramjet to simulate conditions of hypersonic flight at an altitude of 25 km. A sample holder assembly that holds one or more leading edge samples rigidly, without failing after multiple exposures, was inserted into the combustor exhaust stream through an access port in a probe housing at the exit of the combustor section. The assembly was designed and built using an iterative procedure that employed modeling, preliminary trials, and experimental trials as described in Ref. 23

The design used in this work consists of a water-cooled inconel tube with welded sample holder subassemblies all of which were plasma sprayed with a zirconia thermal barrier coating [Fig. 1(a)]. A key aspect of the design is a dovetail slot in the subassemblies to accommodate the 12° included angle of the leading edge (LE) samples. The LE sample was instrumented using a thermocouple that passed through a capillary tube from the back of the water-cooled inconel tube. The thermocouples were spot welded to the back of the inconel tube with nichrome strips in such a way that the tip of the thermocouples firmly contacted the center of the back of the LE samples, hereafter termed the back wall of the LE sample. No attempt was made to attach the thermocouple to the sample or to place it in a machined recess. Thus, accuracy of measurement was sacrificed so as to avoid possible premature failure of the samples. Pyrometric measurement was precluded by the quartz window used in the rig, which has high absorption in the frequency range of interest.

The scramjet rig was operated at different conditions by employing facility nozzles with different Mach numbers, and by varying the vitiator stagnation conditions and combustor's fuel/air equivalence ratio. Parameters of importance for aerothermal effects such as static temperature, static pressure, and total temperature were collected from prior calibrations of the rig. Samples of UHTC and SiC were exposed to different conditions. The total temperature was used to calculate an effective Mach number for free flight at an altitude of 25 km using the equations given in Ref. 1

$$M = U/\sqrt{\gamma R T_1} \tag{1}$$

$$T_t = T_1\left(1 + \frac{\gamma - 1}{2}M^2\right) \tag{2}$$

where U is the fluid velocity, R the individual gas constant for air (286.9 J/kg-K), T_1, T_t the static and total/stagnation

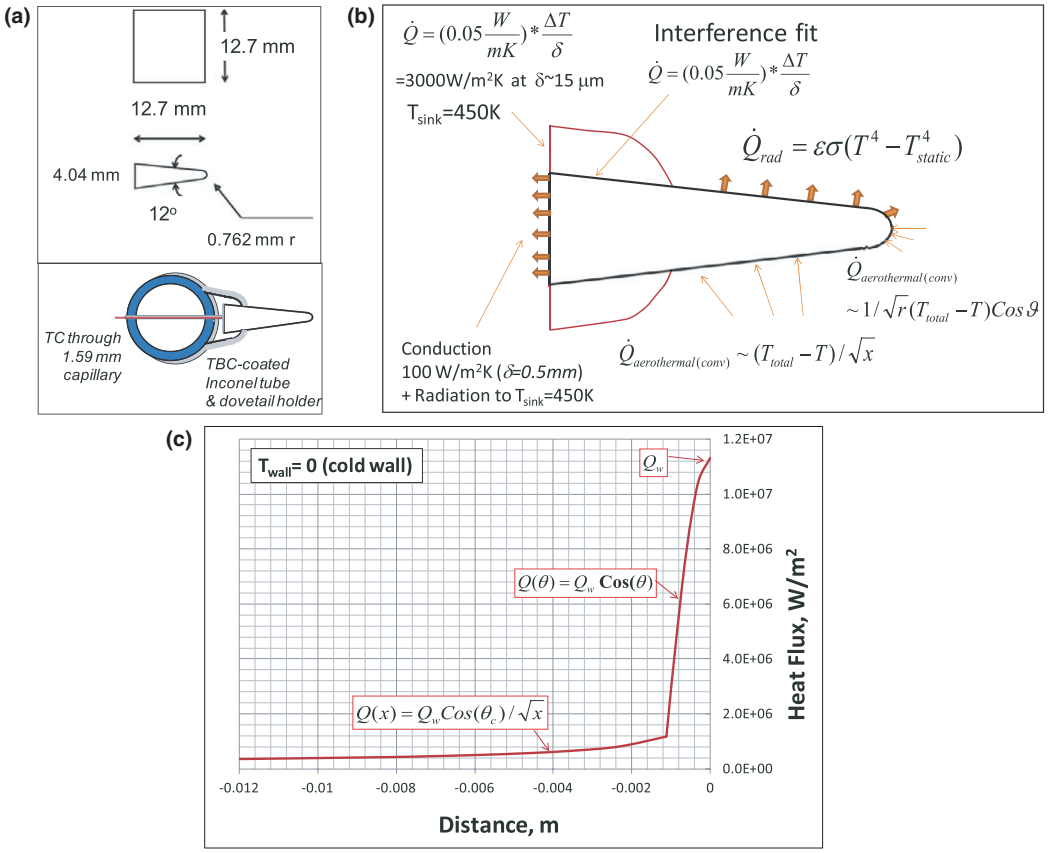

Fig. 1. (a) Schematic sketch of the Leading Edge sample, and the sample holder used in this work. (b) Schematic of thermal loads on the leading edge sample tested in the scramjet. (b) The variation in aerothermal convective heat flux with location along the surface of the leading edge shown for T_{wall} = 0 (cold wall) for effective Mach 6.5 at an altitude of 25 km.

temperatures, respectively, M the mach number and γ the ratio of specific heats of air; the static temperature as a function of altitude was obtained from the standard atmospheric table.[35] The combustor exit gases have characteristics that reproduce nearly the same heat flux, total temperature, fluid velocity, total pressure behind the bow shock as are experienced behind the bow shock under hypersonic flow at an altitude of 25 km, as shown in prior work.[23] The effective Mach numbers for each condition of tests reported in this work are calculated from the total temperature using Eq. (2). The temperatures of the back wall of the samples were continually monitored during the runs using thermocouples. The samples were removed from the holder and examined by optical macroscopy (Nikon D100, Nikon Inc., Melville, NY), scanning electron microscopy (FEI Quanta MkII, FEI Inc., Hillsboro, OR) energy dispersive spectroscopy, EDS (for preliminary analysis) and electron microprobe analysis (CAMECA SX100, Cameca Instruments Inc., Madison, WI) to determine the thickness and chemistry of the scales that formed on them as a function of location from the tip of the sample. X-ray diffraction (Rigaku D/MAX B, RU-200BH, Rigaku Americas, Allison Park, PA) was performed on the scales formed on the slant sides of the leading edge samples to identify phases present.

III. Models

(1) Thermal Response

Interpretation of the experimentally observed data required a model as the thermal profile of the samples from the front to back could not be measured directly during the run. Due to thermal expansions and vibrations present during the run, it was not possible to ensure good thermal contact between the thermocouple and the back wall of the samples. Thus, modeling the thermal response was essential to interpret the data. The model was also helpful in evaluating the effectiveness of the rig in simulating thermal profiles that are similar to what might be present during free flight.

The thermal responses of the scramjet rig samples as well as those that might be experienced in free flight were computed using a finite element model (FEM, Abaqus 6.11, Dassault Systems, Waltham, MA) that incorporated orientation and distance-dependent aerothermal heating, radiative heat flux from the sample to the atmosphere, and conduction within the sample. For the simulation of free-flight conditions, leading edge bodies of dimensions 50.8 mm × 50.8 mm were used with adiabatic conditions at the back wall. For the scramjet samples, the actual dimensions of the samples (12.7 mm × 12.7 mm) were used, along with appropriate thermal boundary conditions for the back end of the sample, as shown in Fig. 1(b). As specified in Fig. 1(b), the boundary conditions at the gripped end assumed that the thermal conductivity of air was 0.05 W/mK, that a gap of 15 micrometer exists at the bolted interface, and a 0.5 mm gap exists between the sample and the dovetail sample holder, based on best estimates of real conditions.

The convective aerothermal heat flux at the leading edge tip was computed from expressions for aerothermal heat flux given in the work of Zoby.[36] Thus the aerothermal heat flux is given by

$$\dot{Q}_{\mathrm{w}}, \mathrm{W/m^2} = 3.88 \times 10^{-4} \sqrt{\frac{p_{t2}(Pa)}{r(m)}} (h_{\mathrm{aw}} - h_{\mathrm{w}}) \tag{3}$$

$$(h_{\mathrm{aw}} - h_{\mathrm{w}}), \mathrm{kJ/kg} = C_{\mathrm{p}}(T_{\mathrm{t}} - T_{\mathrm{wall}}) \tag{4}$$

where $\dot{Q}_{\mathrm{w}}$ is the stagnation heat flux on the material, p_{t2} is the total pressure behind the bow shock, r the radius of curvature of the cylindrical sample, h_{aw} the adiabatic wall enthalpy, h_{w} the enthalpy of air calculated at the material wall temperature, C_{p} the specific heat of air, T_{t} the total temperature, and T_{wall} the material wall temperature. For Mach numbers of up to 7, the degree of dissociation is negligible (<1%) for both O_2 and N_2, as calculated using the expressions given by Scala and Gilbert[37] as shown in Ref. 23 The stagnation or total pressure behind the bow shock, p_{t2}, is given by the Raleigh pitot tube formula:

$$p_{t2} = p_1 \left(\frac{\gamma+1}{2}\right)^{\frac{\gamma}{\gamma-1}} \left(\frac{(\gamma+1)M^2}{2\gamma M^2 - (\gamma-1)}\right)^{\frac{1}{\gamma-1}} M^2 \tag{5}$$

where p_1 is the free stream (static) pressure obtained from prior calibrations of the rig, as detailed in Ref. 23 Note that the heat flux varies with wall temperature and this is accounted for in the FEM model. The heat flux also varies with distance away from the tip due to a change in the orientation of the surface normal with flow, and is given by:

$$\dot{Q}(\theta) = \dot{Q}_w \mathrm{Cos}(\theta) \tag{6}$$

where θ is the orientation of the plane normal relative to the hypersonic flow direction, which varies from 0° at the tip of the LE and reaching θ_c (=84°) as the curvature meets the slant surface. With further distance along the wedge surface at constant, θ_c, the heat flux drops as

$$\dot{Q}(x) = \dot{Q}_w \mathrm{Cos}(\theta_c)/\sqrt{x} \tag{7}$$

where x is the distance from the point where the LE curvature meets the slant surface (the tangent point). A plot of this variation in heat flux is shown in Fig. 1(c) for $T_{\mathrm{wall}} = 0$ (cold wall) for an effective free stream Mach number of 6.5 at an altitude of 25 km. It must be noted that while this distribution in flux includes the correct dependencies, it is an approximation of the actual distribution, especially the transition from angular dependence [Eq. (6)] to distance dependence [Eq. (7)]. The radiative heat flux from the surface to ambient is given by the Stefan-Boltzmann law as shown in Fig. 1(b). It varies with material surface temperature and ambient static temperature. The transient conduction within the sample is solved using the finite element model. The thermal conductivity of the interface between the sample and sample holder was estimated using the conductivity of air (0.05 W/mK) and an estimated gap thickness, as shown in Fig. 1(b). The back wall heat flux was estimated using the conductivity of air across a static air gap and radiation to the water-cooled inconel maintained at an estimated temperature of 450 K. The results at the tip and hotter regions of the sample were not sensitive to the back wall heat conduction estimates. For the simulation of free-flight conditions, the convective aerothermal heat flux was applied to the entire slant surface, and an adiabatic condition was assumed for the back wall.

The conditions in the rig such as total temperature, static temperature, fluid flow velocity, static pressure, and the specific heat ratio of the gas, were obtained from prior calibrations of the scramjet rig. Note that the radiation to the ambient in the scramjet rig is dependent on the static temperature present in the rig, but in the free-flight simulation it depends on the ambient temperature at an altitude of 25 km, taken from standard atmospheric tables.

(2) Oxidation Response

The oxidation response was evaluated using electron microscopy, energy dispersive spectroscopy (EDS), electron probe microanalysis (EPMA), and X-ray diffraction (XRD), as mentioned earlier. The resulting data were interpreted by comparing the scale thicknesses to those predicted by an oxidation model developed based on oxidation experiments conducted in furnace tests. The model used in this work is

detailed elsewhere.[32] The model was found to predict results from furnace tests reasonably well at lower temperatures (up to 1773 K). It was found to underpredict slightly the oxidation rates at higher temperatures, partly due to possible contamination from the high-temperature furnaces used. Furthermore, the model was found to significantly underestimate the oxidation rates in arc jet tests, where the enthalpy is carried by dissociated gases which recombine at the material surface. The model accounts for the high fluid velocity of the ambient present behind the bow shock through boundary layer evaporation. The model does not include the shear stresses that might strip the liquid layer, but under the conditions of the test the model predicts the evaporative flux to be so high that an external glassy layer barely forms. It is thus applicable for the scramjet conditions used in this work. As mentioned earlier, gas dissociation and recombination is not significant at Mach numbers below 7, based on calculations using equations given by Scala and Gilbert.[37] The model predictions for oxide layer thickness were compared with those obtained using the scramjet rig tests. The predictions were based on thermal responses calculated for the tip of the leading edge, using the FEM model detailed earlier.

IV. Results

(1) Experimental Results

A summary of all the runs where LE samples survived are shown in Table I. The conditions of the run were obtained from the data collected during the run and using prior calibrations of the rig. These data were converted using appropriate equations to calculate the cold wall heat flux on the leading edge of the sample which had a 762 micrometer radius of curvature.(see Ref. 5 for details) The dynamic pressure, total pressure, and fluid velocity behind the shock were other parameters used for this evaluation. By comparing to the total temperatures during free flight at an altitude of 25 km, the conditions in the rig were converted to an effective Mach number. Figure 2 shows a plot of sample survival conditions (total temperature and effective Mach numbers) for the UHTC and SiC samples tested. UHTC samples were found to survive more often than SiC samples. The inset shows video captures taken before, during, and after a typical run. For comparison, it must be noted that a graphite sample tested during one of the runs (run ID#10-6 in Table I) burned at a Mach number of 4.7 (using vitiator but no combustion) after nearly 5 min of hold.

Figures 3(a) and (b) show SEM images of the oxide scales formed on the UHTC samples for a typical run (9.3 min at a total temperature of 1550 K, followed by13.3 min at total temperature of 1850 K, runs #10-1 + #10-2) as a function of the location of the leading edge surface with respect to the tip. Figure 3(c) shows the X-ray diffraction pattern obtained on one of the slant sides of the wedged sample. It shows the presence of both hafnia (HfO_2) and hafnon ($HfSiO_4$) in the sample. Figure 4 shows a higher magnification of the scale formed on a leading edge sample after a different run (4.33 min at a total temperature of 1900 K followed by 1.33 min at 2370 K). The figure includes EPMA results collected on two different regions of the scale showing regions of Hf–Si–O and Hf–O. Different filters were used to identify different elements as Si and Hf peaks overlap on EDS maps. From microprobe (EPMA) analyses of the different regions, combined with the XRD data, the scale was found to be comprised mostly of hafnia, with an outer layer containing hafnon. Thus, from the SEM images, EPMA of different regions, and XRD of the scales, the oxide scales were found to contain hafnia and hafnon, with limited presence of silica, but no external glassy layer. There was no SiC-depleted region beneath the oxide scale. In contrast to UHTC samples, no scale was found on the SiC samples that survived. This could result from either high shear stresses or high evaporation rates both arising from the high flow rate conditions. This is consistent with the observation that the surfaces of the scales on UHTC samples were free of silica and the inside of the scale was lean in silica. The formation of hafnon, the lack of an external glassy layer and the lack of silica in the outer regions of the oxide scale are features unique to scramjet testing, presumably due to the high fluid flow conditions, which can cause enhanced loss of silica from the surface.

(2) Model Results

Figures 5(a) and (b) show the material thermal properties used in the model. The specific heat data for both SiC and UHTC are well-established.[18,38] The thermal conductivity for sintered SiC is also known with reasonable certainty.[38] The emissivity of UHTC was taken to be 0.75 based on the work by Meng *et al.*[39] and that of SiC to be 0.9. The model results had a very weak dependence on emissivity, but a strong dependence on specific heat and thermal conductivity. The specific heat is well-known, but a large variation in the thermal conductivity for UHTC has been noted in recent works.(see e.g., Ref. 18) Hence the thermal diffusivity of the sample used in this study was measured using laser flash up to a temperature of 1200°C. As shown in Fig. 5(b), this datum converted to thermal conductivity (from specific heat and density) was found to lie very close to an average curve fit to available literature data in Ref. 18 Figure 5(c) shows the typical FEM model results for the calculated thermal response of the UHTC LE samples within the scramjet rig and that of a UHTC LE in free flight. The scramjet sample was simulated using the actual dimensions of the sample (30 mil curvature at the tip, 12° included angle, 12.7 mm × 12.7 mm) and sample holder assembly. The thermal response of an UHTC LE under free-flight conditions was calculated using the same tip curvature and included angle of the wedge, but with a significantly larger sample size of 50.8 mm × 50.8 mm. The back wall of the sample was taken to be adiabatic. From the plot of temperature versus distance from the leading edge tip shown in Fig. 5(d), it is seen that the sample in the scramjet rig has almost the same profile as that in free flight. The LE sample is cooler only in the region where the sample holder grips the sample, as is to be expected. For a free flight of Mach 7, the leading edge reaches a temperature of ~1850 K, and decreases with distance at a rate of ~40 K/mm.

Figure 6 shows the various recorded and predicted temperatures in the rig as a function of effective Mach number for the UHTC and SiC samples. The plot compares the measured back wall temperatures measured during the run, the predicted LE tip temperature from the model, and the predicted back wall temperature from the model. The measured temperatures are slightly below the predicted temperatures, presumably due to the lack of proper contact and effects from thermal expansion and vibrations, as explained earlier. Note that the LE tip temperatures for SiC are predicted to be slightly higher than those for UHTC, and the back wall temperatures lower, quite likely from the lower thermal conductivity of SiC at high temperatures.

Figure 7 shows a comparison of the oxide thicknesses measured using scanning electron microscopy on the LE samples for different runs of UHTC, with the curves predicted by the model. The model predictions included the effects of increased total pressures behind the shock wave, and the high fluid velocity behind the shock wave that the material will experience. Data from furnace or arc jets were not available for the exact temperatures experienced by the leading edge, but data available for temperatures that are close are shown for comparison purposes. In Fig. 7(b), oxide thicknesses measured on samples tested in a furnace near the same temperature is included. Figure 7(d) shows a comparison of UHTC samples tested in a furnace and those tested in an arc jet at the same temperature. The model predicts that

Table I. A List of Runs with Parameters and Calculated Conditions, Under Which Leading Edge Samples Survived Exposures in the Scramjet Rig

RunID No.	Facility Nozzle Mach No.	Vitiator Temp, R	ERratio	Total Temp T_t,K	Total Pressure P_{t2}, atm	Duration (s)	No. of cycles	Total Duration (min)	Samples Survived	SiC Backface Temp, K	UHTC Backface Temp, K	C.W. Heat Flux MW/m^2	Effective Mach#	UHTC oxide Thickness (μm)
10-1	1.8	1200	0.45	1550	1.0	140	4	9.3	SiC, UHTC			7.77	5.5	
10-2	1.8	2000	0.5	1850	1.2	158	5	22.5	SiC, UHTC	900	1100	8.8	6.1	6–11
10-3	2.2	2200	0.6	2100	1.4	80	1		—	900	1100	11.3	6.5	—
10-4	2.2	2200	0.5	1950	1.3	100	1	1.7	UHTC	1050	950	10.1	6.2	5–8
10-5	2.2	1950	0.5	1880	1.4	80	1		SiC, UHTC	1000	900	10.2	6.1	
	2.2	2200	0.5	1900	1.4	80	1		SiC, UHTC	1000	900	10.3	6.2	
	2.2	1950	0.5	1925	1.4	50	1		SiC, UHTC	1000	910	10.4	6.2	
	2.2	1950	0.5	1950	1.4	50	1		SiC, UHTC	1000	915	10.5	6.2	
	2.2	2200	0.8	2350	1.6	40	1		UHTC		1100	13.8	6.9	
	2.2	2200	0.9	2370	1.6	40	1	5.7	UHTC		1100	14	7.0	8–12
10-6	2.2	2200	0	1200	1.1	400	1		UHTC		550	5.5	4.7	
	2.2	2200	0.5	1900	1.4	72	1	7.9	—		1000	10.5	6.2	—
11-1	1.8	1800	0.3	1500	1.0	140	1		UHTC		950	7	5.4	
	1.8	1800	0.5	1820	1.1	128	1		UHTC		975	9	6.0	
	1.8	1800	0.7	2000	1.2	15	1	4.7	—		1000	10	6.3	—
11-2	1.8	1800	0	1000	0.8	300	1		UHTC 1, 2		400	4	4.2	
	1.8	1800	0.3	1500	1.0	60	1		UHTC 1, 2		700	7	5.4	
	1.8	1800	0.5	1800	1.1	30	1		UHTC 1, 2		830	8.8	6.0	
	1.8	1800	0.6	1900	1.2	30	1		UHTC 1, 2		1000	9.5	6.2	
	1.8	1800	0.7	2000	1.2	20	1		UHTC 2		1020	10	6.3	
	1.8	1800	0.8	2080	1.3	20	1		UHTC 2		1030	10.8	6.5	
	1.8	1800	0.9	2180	1.3	15	1	7.9	—		1050	11.5	6.6	—
11-3	1.8	1800	0.6	1910	1.2	150	1		UHTC 1, 2		1000	9	6.2	
			0.6	1910	1.2	210	1	6.0	UHTC1		1000	9	6.2	4–6
11-4	1.8	1800	0.6	1910	1.2	190	3	9.5	UHTC2, UHTC1*		1000	9.75	6.2	5–7
11-5	1.8	1800	0.6	1910	1.2	170	2	15.2	UHTC1*		1100	9.75	6.2	6–8
11-5	1.8	1800	0.6	1910	1.2	170	2	5.7	UHTC2		1100	9.75	6.2	3–7

†* - UHTC1* sample used in run#11-4 was reused in run#11-5.

the evaporation rate of external glass will be sufficiently fast to prevent a stable external glassy film, as experimentally observed.

V. Discussion

This work presents the thermal and oxidation responses of UHTC and SiC leading edge samples exposed to hypersonic flow conditions which simulated effective free flight Mach numbers of 6–7 at an altitude of 25 km. The temperatures reached during the run at the back wall of the sample, which is 12.7 mm (0.5″) from the leading edge, were measured using thermocouples which firmly touched the back wall of the samples at room temperature. The scale thicknesses formed on the samples were characterized using SEM, EDS, EPMA, and XRD. The results were interpreted using a combination of aerothermal, thermal, and oxidation modeling. The following is a discussion of the results.

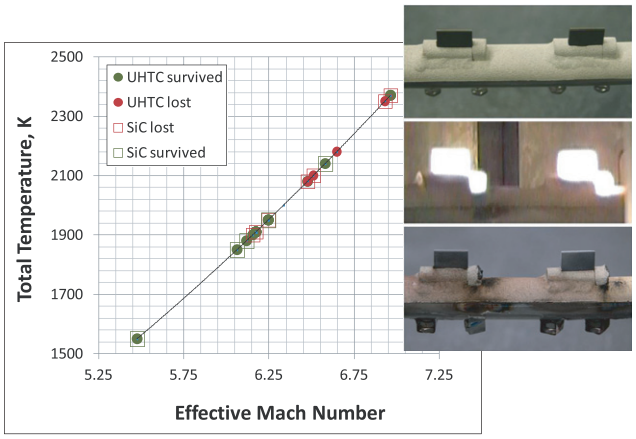

Fig. 2. A plot of conditions under which UHTC and SiC leading edge samples were exposed. The green and red symbols denote conditions where the samples survived or were lost respectively, with circles representing UHTC and squares representing SiC. UHTC samples were found to have a better survival rate than SiC samples. The inset shows video captures before, during and after a typical run.

The scramjet rig conditions vary from run to run, but all the parameters of importance for aerothermal calculations are available either through live recordings of data or prior calibrations to control parameters. The total temperature was used to calculate an effective Mach number for free flight at this altitude. From Fig. 2, it is clear that we can obtain a range of Mach numbers spanning from 5 to 7 under combustion conditions which the UHTC samples are capable of surviving. The thermal modeling results shown in Fig. 5 illustrate that the thermal profile experienced by the 12.7 mm (0.5″) leading edge sample in the rig are very close to that for a much larger 50.8 mm (2″) sample under free-flight conditions.

When combined, the experiments and modeling show that the tip of the UHTC LE sample reaches temperatures far below that of the total temperature. As shown in Fig. 6, the measured and predicted back wall temperatures are much lower than the total temperature and the LE tip temperatures are predicted to be in between the two. For example, it is seen that for UHTC, the LE tip reaches a temperature of 1850 K, when the total temperature is 2380 K and the static temperature in the rig is 1450 K. The same profile is reached in a larger LE of UHTC under free flight conditions of Mach 7 at an altitude of 25 km with a static ambient temperature of 220 K as seen from Fig. 5. Thus, for reusable hypersonic vehicles the maximum temperature reached by a thermal protection system using UHTCs will be 1850 K for up to Mach 7. Two parameters of interest, temperature and heat flux, are often used in test methods to evaluate candidate materials. Figure 8 gives suggested values to be used in such tests for various free-flight conditions. The total temperature and temperature reached at the tip of the LE are shown in Fig. 8(a). The initial cold wall heat flux and steady-state heat flux are

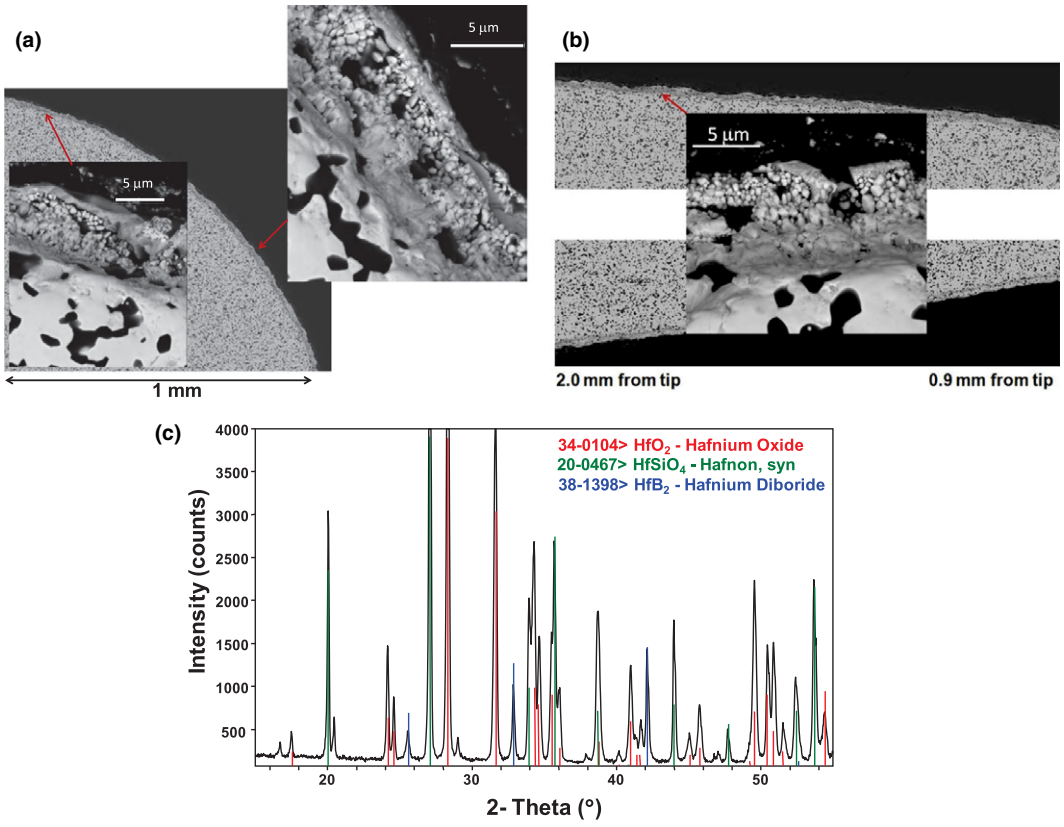

Fig. 3. (a) Oxidation scale at the tip of a UHTC leading edge sample after exposure in the scramjet rig for 9.3 min at a total temperature of 1550 K, followed by13.3 min at total temperature of 1850 K. (b) oxidation scale formed over the slant edges of the 12° wedge away from the leading edge tip. There was no evidence of external glassy layer or internal depletion layer, which have been reported to form in furnace experiments. (c) X-ray diffraction pattern obtained from the slant sides showing presence of hafnia and hafnon in the scale.

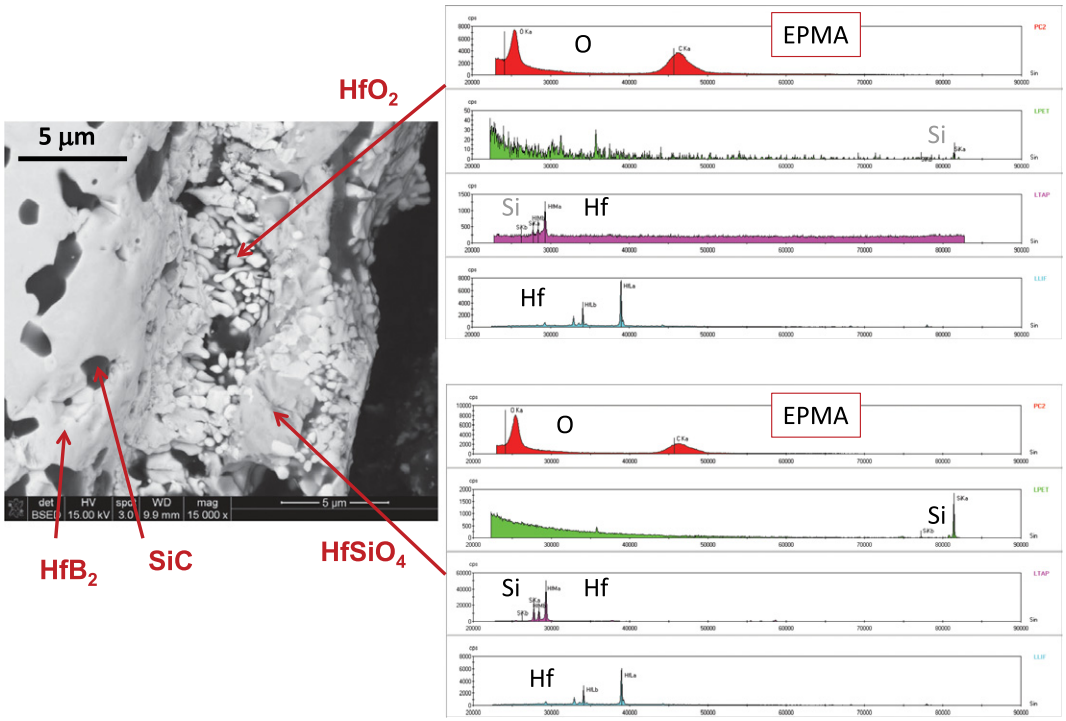

Fig. 4. Oxidation scale at the tip of an UHTC leading edge sample after exposure in the scramjet rig for 4.33 min at a total temperature of 1900 K followed by 1.33 min at 2370 K. There was no evidence of an external glassy layer or internal depletion layer. EPMA analysis of the scale showed the presence of both hafnia and hafnon in the oxide scale. Note that the scale used for Si in the EPMA corresponding to hafnia region is much smaller than that shown for the hafnon region. X-ray diffraction of the scale also showed the presence of both hafnia and hafnon in the scale.

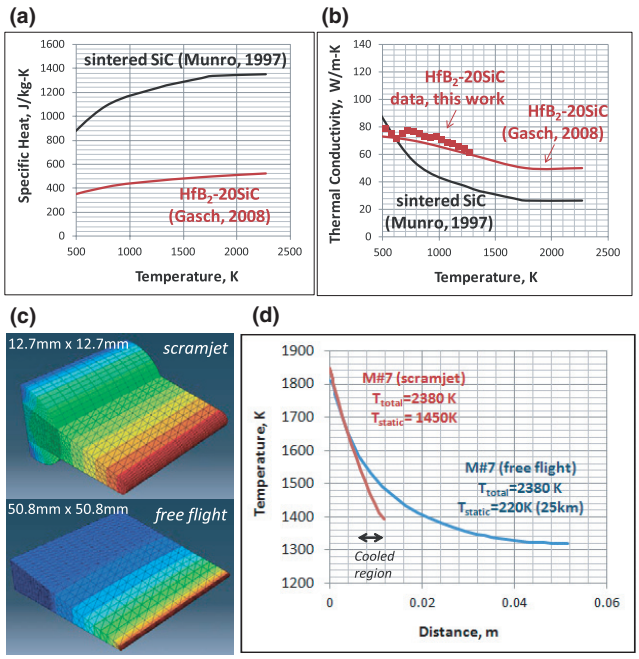

Fig. 5. (a,b) The temperature-dependent thermal properties used in the model were obtained from literature and experimental data on UHTC used in this work. (c,d) The calculated thermal response of the leading edge in the scramjet rig is shown compared with the calculated response of a larger sample in free flight using adiabatic conditions for the back wall. It is seen that the thermal response of the sample in the scramjet rig follows closely that in free flight except for the portion of the sample that is held in the cooled dovetail region.

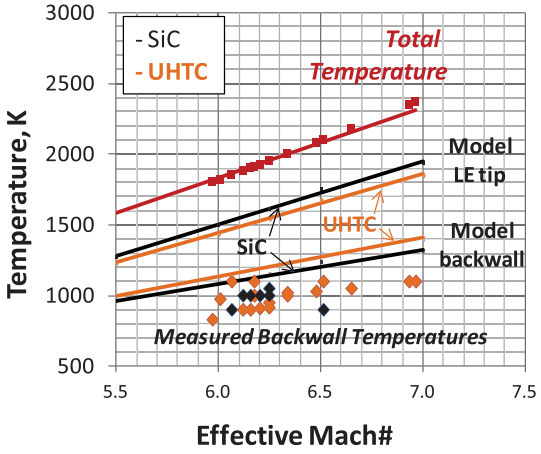

Fig. 6. The various recorded and predicted temperatures for all the runs are shown plotted as a function of effective Mach number of the simulation conditions used in the scramjet rig for UHTC samples and SiC samples. The higher thermal conductivity of UHTC results in lower LE tip temperature than the SiC sanple.

shown in Fig. 8(b). The variation in material temperature with distance from the tip is shown in Fig. 8(c). The scale thickness formed over the LE is shown in Fig. 8(d). Note that the scale thickness does not vary significantly with distance from the tip for short exposures (10 min) consistent with the small variation in scale thicknesses observed on the LE samples as shown in Figs. 3 and 4.

The comparisons of the oxidation model predictions with the experimental data from samples tested in the scramjet show reasonable agreement, but the experimental values are consistently higher than the predicted values by a small margin. This is true for furnace tested samples as well, but only at higher temperatures where contamination from the furnace was thought responsible for the discrepancy.[32] The arc jet tests typically show a larger scale thickness than furnace tests as shown by other investigators and as seen from Fig.8(d) and pointed out in more detail in Ref. 32 One possible reason for the observed higher oxidation rates in the

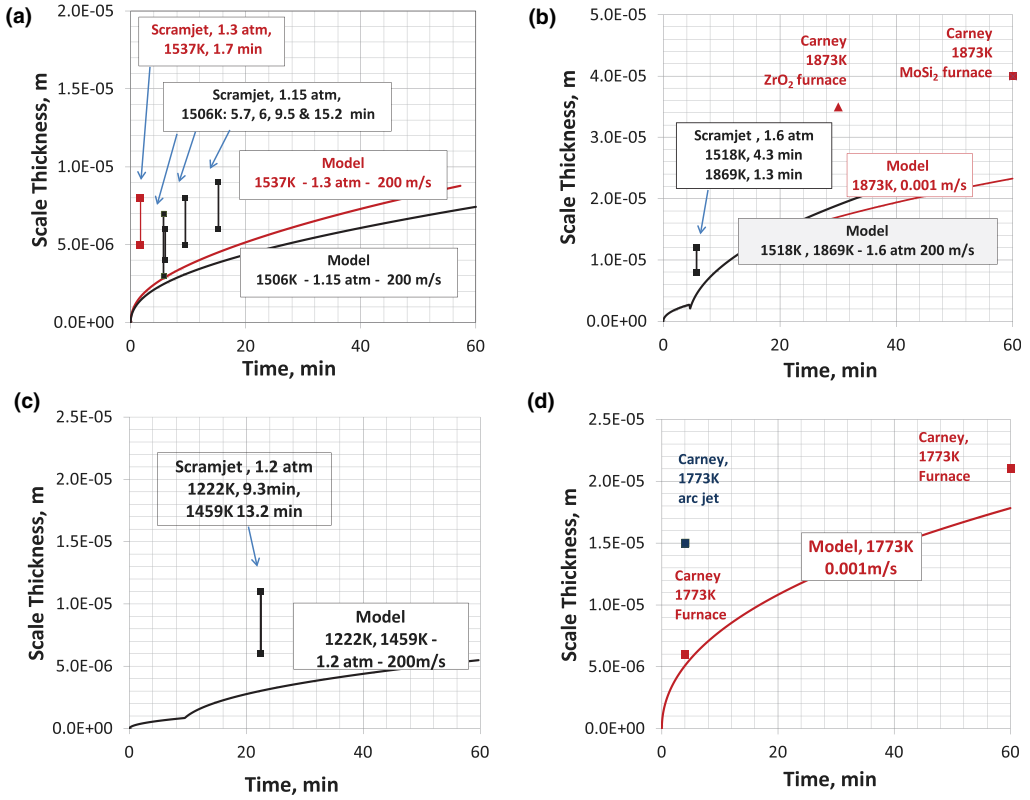

Fig. 7. The oxidation scale thicknesses measured on the LE samples after exposures in the scramjet rig are shown plotted with model predictions, furnace oxidation data, and arc jet oxidation data. The scales on the LE samples are slightly thicker than model predictions using the predicted material temperatures, but not very different from the trends in how the model compares with the furnace data at high temperatures. On the contrary, the arcjet data is considerably larger than both.

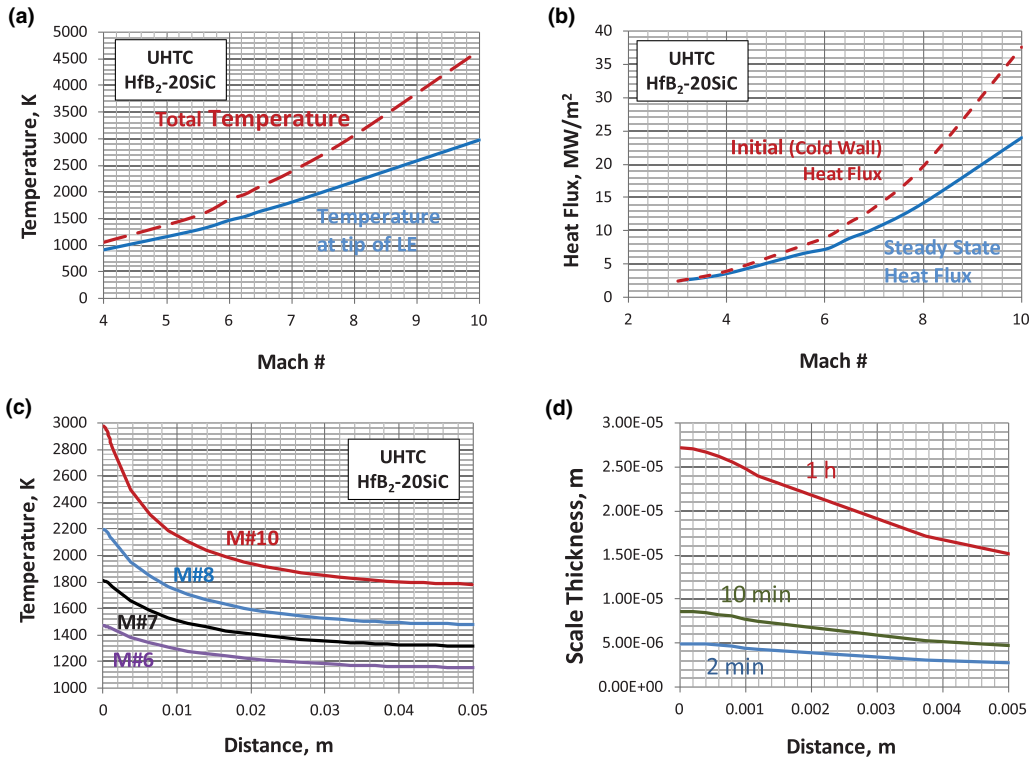

Fig. 8. Calculated thermal response of UHTC as leading edge, plotted as a function of effective free stream Mach number at an altitude of 25 km. (a) Total and material tip temperatures, (b) Cold wall and steady state heat flux, (c) temperature profiles with distance from the tip of the LE, and (d) predicted thickness of oxide scale as a function of distance from the LE tip for 2 min, 10 min and 1 h at a free-flight simulation of Mach 7. Note that at short durations, the scale thickness does not vary significantly with distance, rationalizing the experimental observations (Fig. 3 and 4).

scramjet compared to the model prediction even at lower temperatures is that the chemistry of the scramjet fluid includes significant moisture. The other possible reason could arise from the observation of the formation of hafnon in the scale which would result in volume shrinkage making the scale open up the pore fraction. Finally much less glassy

phase was found on the scale compared to the samples tested in the furnace. It is believed that the hypersonic flow is able to evaporate or pull the glassy material out of the scale thus resulting in a porous oxide scale with no glassy phase filling it, at least at the outer most regions of the scale. Further characterization of the scales will be required to understand the mechanisms contributing to the slightly enhanced oxidation under the scramjet and arc jet conditions. Despite these limitations, the model captures the dependencies well and predicts oxidation rates within reasonable error for use in engineering design.

VI. Summary

Sharp leading edge samples of UHTC (20 vol%SiC–HfB2) and SiC were exposed to simulated hypersonic free-flight conditions using the post combustion section of a direct-connect scramjet rig, which served effectively as a hypersonic wind tunnel. The UHTC samples survived more often than SiC samples and withstood exposures for up to 15 min under conditions that simulated free flight at an altitude of 25 km at Mach 6.25, and survived a 80 s exposure at Mach 7. The measured back wall temperatures were far below the total temperatures and the oxidation scales were thinner than what might be expected to form at total temperatures. These results were rationalized using a combination of thermal and oxidation models. The tip of the LE samples reached temperatures calculated to be 350–500 K below the total temperatures and maintained a steep gradient of 40 K/mm away from the tip, at steady state. Similarly the steady-state heat fluxes were 15%–20% below the cold wall heat fluxes. The thermal model predicted that for the same conditions, the tip temperature for UHTC was lower than that for SiC due to the higher thermal conductivity of UHTC at temperature. The scale thicknesses on UHTCs were within reasonable limits of predictions from the oxidation model. Possible reasons for slightly enhanced oxidation in the scramjet compared to the model are likely due to the formation of hafnon in the scale and the impurities in the scramjet environment including higher moisture content. The scale thicknesses were similar to values reported for exposures in furnaces but less than those reported in arc jet tests. The absence of an external glassy layer and absence of silica in the outer portions of the oxide region are unique to samples tested in the scramjet, presumably due to the high fluid flow rates.

Acknowledgments

We acknowledge significant support from Charles Smith, Jerry Malott, Ken Sack and Andrew Baron of ISSI, Dayton, OH and Steve Smith of AFRL/RQHF, WPAFB, OH, all of whom operated the scramjet rig with dedication and offered creative suggestions. This work was supported by USAF Contract # FA8650-10-D-5226 which included funding from US Air Force Office of Scientific Research (AFOSR), monitored by Dr. Ali Sayir.

References

[1]Ames Research Staff, "Equations, Tables and Charts for Compressible Flow"; National Advisory Committe for Aeronautics [Report 1135] 1953.

[2]L. Lees, "On the Boundary Layer Equations in Hypersonic Flow and Their Approximate Solutions," *J. Aero. Sci.*, **20** [2] 143–5 (1953).

[3]J. A. Fay and F. R. Riddell, "Theory of Stagnation Point Heat Transfer in Dissociated Air," *J. Aero. Sci.*, **25**, 73–85 (1958).

[4]M. M. Opeka, I. G. Talmy, and J. A. Zaykoski, "Oxidation-Based Materials Selection for 2000°C+ Hypersonic Aerosurfaces: Theoretical Considerations and Historical Experience," *J. Mater. Sci.*, **39**, 5887–904 (2004).

[5]E. Wuchina, M. Opeka, S. Causey, K. Buesking, J. Spain, A. Cull, J. Routbort, and F. Guitierrez-Mora, "Designing for Ultrahigh-Temperature Applications: The Mechanical and Thermal Properties of HfB_2, HfC_x, HfN_x and a-Hf(N)," *J. Mater. Sci.*, **39**, 5939–49 (2004).

[6]F. Montverde and R. Savino, "Stability of Ultra-High-Temperature ZrB_2–SiC Ceramics Under Simulated Atmospheric re-Entry Conditions," *J. Eur. Ceram. Soc.*, **27**, 4797–805 (2007).

[7]E. J. Opila and M. C. Halbig, "Oxidation of ZrB_2-SiC," *Ceram. Eng. Sci. Proc.*, **22** [3] 221–8 (2001).

[8]F. Monteverde and A. Bellosi, "Oxidation of ZrB_2-Based Ceramics in Dry Air," *J. Electrochem. Soc.*, **150** [11] B552–9 (2003).

[9]W. G. Fahrenholtz, G. E. Hilmas, A. L. Chamberlain, and J. W. Zimmermann, "Processing and Characterization of ZrB_2-Based Ultra-High Temperature Monolithic and Fibrous Monolithic Ceramics," *J. Mater. Sci.*, **39** [19] 5951–7 (2004).

[10]E. Opila, S. Levine, and J. Lorincz, "Oxidation of ZrB_2- and HfB_2-Based Ultra-High Temperature Ceramics: Effect of Ta Additions," *J. Mater. Sci.*, **39**, 5969–77 (2004).

[11]F. Monteverde, "Progress in the Fabrication of Ultra-High-Temperature Ceramics: "In Situ" Synthesis, Microstructure and Properties of a Reactive Hot-Pressed HfB_2–SiC Composite," *Composite Sci & Tech.*, **65**, 1869–79 (2005).

[12]X.-H. Zhang, P. Hu, and J.-C. Han, "Structure Evolution of ZrB_2-SiC During the Oxidation in Air," *J. Mater. Res.*, **23** [7] 1961–72 (2008).

[13]M. Wang, C.-A. Wang, L. Yu, Y. Huang, and Z. Zhang, "Oxidation Behavior of SiC Platelet-Reinforced ZrB_2 Ceramic Matrix Composites," *International J. App. Ceram. Tech.*, **9** [1] 178–85 (2012).

[14]C. M. Carney, "Oxidation Resistance of Hafnium Diboride-Silicon Carbide from 1400-2000C," *J. Mater. Sci.*, **44**, 5673–81 (2009).

[15]C. M. Carney, P. Mogilevsky, and T. A. Parthasarathy, "Oxidation Behavior of Zirconium Diboride Silicon Carbide Produced by the Spark Plasma Sintering Method," *J. Amer. Ceram. Soc.*, **92** [9] 2046–52 (2009).

[16]D. D. Jayaseelan, H. Jackson, E. Eakins, P. Brown, and W. E. Lee, "Laser Modified Microstructures in ZrB_2, ZrB_2/SiC and ZrC," *J. Eur. Ceram. Soc.*, **30** [11] 2279–88 (2010).

[17]Y. Wang, X. Zhu, L. Zhang, and L. Cheng, "Reaction Kinetics and Ablation Properties of C/C–ZrC Composites Fabricated by Reactive Melt Infiltration," *Ceram. Int.*, **37** [4] 1277–1283 (2011).

[18]M. Gasch and S. Johnson, "Physical Characterization and Arcjet Oxidation of Hafnium-Based Ultra High Temperature Ceramics Fabricated by Hot Pressing and Field-Assisted Sintering," *J. Eur. Ceram. Soc.*, **30**, 2337–44 (2010).

[19]R. Savino, M. D. S. Fumo, D. Paterna, A. D. Maso, and F. Monteverde, "Arc-jet Testing of Ultra-High-Temperature-Ceramics," *Aerosp. Sci. Technol.*, **14**, 178–87 (2010).

[20]F. Monteverde and R. Savino, "ZrB_2-SiC Sharp Leading Edges in High Enthalpy Supersonic Flows," *J. Amer. Ceram. Soc.*, **95** [7] 2282–9 (2012).

[21]F. Montverde, R. Savino, and M. Fumo, "Dynamic Oxidation of Ultra-High Temperature ZrB_2–SiC Under High Enthalpy Supersonic Flows," *Corros. Sci.*, **53**, 922–9 (2011).

[22]R. T. Voland, L. D. Huebner, and C. R. McClinton, "X-43A Hypersonic Vehicle Technology Development," *Acta Astronaut.*, **59**, 181–91 (2006).

[23]T. A. Parthasarathy, M. D. Petry, G. Jefferson, M. K. Cinibulk, T. Mathur, and M. R. Gruber, "Development of a Test to Evaluate Aerothermal Response of Materials to Hypersonic Flow Using a ScramjetWind Tunnel," *Int. J. Appl. Ceram. Tech.*, **8** [4] 832–47 (2011).

[24]D. J. Thomas, "Design and Analysis of UHTC Leading Edge Attachment"; NASA tech report, NASA/CR-2002-211505 2002.

[25]R. Savino, M. D. S. Fumo, D. Paterna, and M. Serpico, "Aerothermodynamic Study of UHTC-Based Thermal Protection Systems," *Aerospace Sci. Tech.*, **9**, 151–60 (2005).

[26]W. G. Fahrenholtz, "Thermodynamic Analysis of ZrB_2–SiC Oxidation: Formation of a SiC-Depleted Region," *J. Amer. Ceram. Soc.*, **90** [1] 143–8 (2007).

[27]T. A. Parthasarathy, R. A. Rapp, M. Opeka, and R. J. Kerans, "A Model for the Oxidation of ZrB_2, HfB_2 and TiB_2," *Acta Mater.*, **55**, 5999–6010 (2007).

[28]W.-B. Han, P. Hu, X.-H. Zhang, J.-C. Han, and S.-H. Meng, "High-Temperature Oxidation at 19001C of ZrB_2–XSiC Ultrahigh-Temperature Ceramic Composites," *J. Amer. Ceram. Soc.*, **91** [10] 3328–34 (2008).

[29]S. N. Karlsdottir and J. W. Halloran, "Oxidation of ZrB_2-SiC: Influence of SiC Content on Solid and Liquid Oxide Phase Formation," *J. Amer. Ceram. Soc.*, **92** [2] 481–6 (2009).

[30]J. Marschall, D. A. Pejakovic, W. G. Fahrenholtz, G. E. Hilmas, S. Zhu, J. Ridge, D. G. Fletcher, C. O. Asma, and J. Thomel, "Oxidation of ZrB_2–SiC Ultrahigh-Temperature Ceramic Composites in Dissociated Air," *J. Thermophys. Heat Transfer*, **23** [2] 267–78 (2009).

[31]S. Gangireddy, S. N. Karlsdottir, and J. W. Halloran, "Liquid Oxide Flow during Oxidation of Zirconium Diboride-Silicon Carbide Ultra High Temperature Ceramics," *Key Eng. Mater.*, **434–435**, 144–8 (2010).

[32]T. A. Parthasarathy, R. A. Rapp, M. Opeka, and M. K. Cinibulk, "Modeling Oxidation Kinetics of SiC-Containing Refractory Diborides," *J. Amer. Ceram. Soc.*, **95** [1] 338–49 (2012).

[33]M. Gruber, J. Donbar, K. J. Jackson, T. Mathur, R. Baurle, D. Eklund, and C. Smith, "Newly Developed Direct-Connect High-Enthalpy Supersonic Combustion Research Facility," *J. Propul. Power*, **17** [6] 1296–304 (2001).

[34]M. Gruber, S. Smith, and T. Mathur, "Experimental Characterization of Hydrocarbon-Fueled Axisymmetric Scramjet Combustor Flowpaths"; AIAA Paper 2011-2311 2011.

[35]NASA, "U S Standard Atmosphere"; NOAA document ST 76-1562 1976.

[36]E. V. Zoby, "Empirical Stagnation-Point Heat-Transfer Relation in Several Gas Mixtures at High Enthalpy Levels"; NASA tech note, NASA TN D-4799 1968.

[37]S. M. Scala and L. M. Gilbert, "Theory of Hypersonic Laminar Stagnation Region Heat Transfer in Dissociating Gases"; NASA tech note NAS 7-100 Accession No. N71-70918 1963.

[38]R. G. Munro, "Material Properties of Sintered a-SiC," *J. Phys. Chem. Ref. Data*, **26** [5] 1195–203 (1997).

[39]S. Meng, H. Chen, J. Hu, and Z. Wang, "Radiative properties characterization of ZrB2–SiC-based ultrahigh temperature ceramic at high temperature," *Mater. Des.*, **32**, 377–81 (2011). □